



Seismic Rock Physics of Gas-Hydrate Bearing Sediments

4

Davide Gei, José M. Carcione, and Stefano Picotti

Abstract

We describe a methodology to estimate the seismic velocities and attenuation of gas-hydrate bearing sediments as a function of the differential pressure and partial saturation. The model is based on a generalization of the Biot theory of poroelasticity, considering two solids (sediment grains and clathrate hydrate) and two immiscible fluids (water and gas). The rock frames depend on the effective pressure and stiffening for increased hydrate concentration and is accounted for with a percolation model. The fluid effects are modeled with empirical mixing laws characterizing the effective viscosity and fluid bulk modulus as a function of saturation and frequency. Attenuation is described with a constant-Q model and high frequency viscodynamic effects. The model predicts the behavior of real sediments in many respects: (1) velocity increases considerably at high frequencies due to an empirical mixing law of the fluid moduli, taking into account patchy saturation, (2) there is a strong decrease in the wet-rock velocity and Q-factor with decreasing effective pressure, as the dry-rock moduli are highly affected, (3) the dissipation factor has a maximum value at the Biot relaxation peak, ranging from sonic frequencies for full gas saturation to ultrasonic frequencies with a peak value around 40% water saturation, (4) in general, velocity increases and attenuation decreases with increasing gas-hydrate concentration, (5) the S-wave velocity increases with frequency and gas saturation as a consequence of the decreasing bulk density, while S-wave attenuation shows a maximum at full water saturation, at the approximate location of the Biot peak and (6) both velocity and attenuation increase

and decrease for increasing effective pressure. We apply this theory to sediments from the ODP Leg 146 site 892, Oregon accretionary prism.

4.1 Introduction

Reflection seismic is one of the most efficient geophysical methods for investigating subsoil structures and the acoustical properties of sediments, which depend on the composition of solid particles, fluid saturation (water and gas) and on the mechanisms of interaction of the different components.

In this article, we describe a three-phase Biot (TPB) theory to model wave propagation in gas-hydrate bearing sediments. Leclaire et al. (1994) generalized the Biot theory (Biot 1956, 1962) to partially frozen sediments. The model considers two solid frames and one fluid and can be applied to both unconsolidated and consolidated media. Carcione and Tinivella (2000) generalized Leclaire's theory by introducing contact between the grains and the hydrate in the computation of potential and kinetic energies. Moreover, they included the contribution of grain cementation as it affects the elastic properties of the rock matrix. Gei and Carcione (2003) considered the effects of pore pressure and partial saturation (gas and water), incorporating attenuation at all frequencies from the seismic to the ultrasonic band. Therefore, the TPB theory allows for the coexistence of water and free gas in the porous space, which has been reported in several studies (e.g. Milkov et al. 2004; Qian et al. 2018; Sahoo et al. 2018).

This theory is quite general in the sense that there are no assumptions about the shape of the pores and grains, and the limitations are those of the Biot theory (see Carcione 2014; Chap. 7). The description of anelasticity can be improved by incorporating the mesoscopic patchy-saturation effects based on the White model (or similar) and the squirt-flow

D. Gei (✉) · J. M. Carcione · S. Picotti
National Institute of Oceanography and Applied Geophysics -
OGS, Sgonico, Italy
e-mail: dgei@inogs.it

mechanism (Carcione and Gurevich 2011; Sects. 7.12 and 7.13 in Carcione 2014; Carcione et al. 2018).

This article is divided into three main parts. First, we describe the theoretical approach in determining the different parameters involved in the theory, such as the dry-rock moduli, the properties of the fluid mixture, the permeabilities and the quality factors. Then, we provide the equations to compute the P- and S-wave velocities and attenuation. Finally, we present an example illustrating the application of the model to a real case study.

4.2 Dry-Rock Moduli

The elastic properties of the rock and hydrate frames can be computed with theoretical or empirical relationships. However, calibration with experimental data is necessary to evaluate the influence of pore pressure on the properties of the frames to estimate the seismic velocities and attenuation.

4.2.1 Elastic Moduli from Theoretical Models

We denote the sediment grain, hydrate, water, gas and fluid mixture with the subscripts “s”, “h”, “w”, “g” and “f”, respectively. In a partially saturated, gas-hydrate bearing rock, the following relationship holds $\phi_s + \phi_h + \phi_w + \phi_g = 1$, where the terms of the sum are the volume fractions of the different components and the rock porosity is $\phi = \phi_w + \phi_g + \phi_h$. The hydrate concentration is given by $C_h = \phi_h/\phi$, while the saturation refers to the pore space not occupied by the solid phases, i.e. the water and gas saturations are $S_w = \phi_w/(\phi - \phi_h)$ and $S_g = \phi_g/(\phi - \phi_h)$, respectively, with $S_w + S_g = 1$. The proportion of the fluid phase in the rock is $\phi_f = \phi_w + \phi_g$.

The bulk and shear moduli of the rock frame (K_{sm} , μ_{sm}) are obtained with the model proposed by Krief et al. (1990)

$$K_{sm} = K_s(1 - \phi)^{A/(1-\phi)}, \mu_{sm} = K_{sm}\mu_s/K_s, \quad (4.1)$$

where K_s and μ_s are the elastic moduli of the particles forming the sediment and A is an empirical coefficient. Krief et al. (1990) considered a value of $A = 3$, regardless the lithological composition of the sediments. In the case of a multi-mineral rock, the effective K_s and μ_s are obtained with the average Hashin-Strikman bounds (Hashin and Shtrikman 1963; Carcione et al. 2005; Mavko et al. 2009) and the density of the effective solid is $\rho_s = \sum_i S_i \rho_i$, where $S_i = \phi_i/(1 - \phi)$ is the volume fraction of the i th mineral phase and ρ_i is its density. On the other hand, the elastic moduli of the hydrate frame are obtained as (Leclaire et al. 1994).

$$K_{hm} = K_{hmKT}(\phi_h/\phi)^{3.8}, \text{ and } \mu_{hm} = \mu_{hmKT}(\phi_h/\phi)^{3.8}, \quad (4.2)$$

where ϕ_h is the volumetric gas-hydrate fraction and K_{hmKT} and μ_{hmKT} are elastic moduli obtained with the Kuster and Toksöz theory (Kuster and Toksöz 1974; Mavko et al. 2009), considering a solid made of hydrate with air in spherical pores and porosity $\phi' = 1 - \phi$.

We assume that gas hydrate crystallization in the porous space causes stiffening of the skeleton, described by (Carcione and Tinivella 2000)

$$\mu_{smh} = \mu_{sm} + (\mu_{smKT} - \mu_{sm})(\phi_h/\phi)^p, \quad (4.3)$$

where p is the percolation coefficient and μ_{smKT} is the rigidity of the sediment in the absence of a hydrate. The shear modulus μ_{smKT} is obtained with the Kuster and Toksöz theory considering air in the pores. Arbabi and Sahimi (1988) found that $p = 3.8$ with an error of 3%, when computing the elastic properties of three-dimensional percolation networks with the Monte-Carlo technique and finite-size scaling analysis.

4.2.2 Dry-Rock Elastic Moduli from Calibration

The elastic moduli of the rock frame $K_{sm}(z)$ and $\mu_{sm}(z)$ can be computed with Eq. (4.1) if the porosity $\phi(z)$ from log data, not affected by the presence of hydrate, is available. The mineralogical composition of the rock must also be available, and the empirical coefficient A can be estimated from regional data of the study area. Alternatively, if log data of velocity, porosity, rock composition, bulk density and saturation are available, $K_{sm}(z)$ and $\mu_{sm}(z)$ can be obtained with the inverse Gassmann equation (e.g. Carcione 2014; Mavko et al. 2009), considering log sections without gas hydrate.

The acoustic and transport properties of a rock depend on the effective pressure as

$$p_e = p_c - np, \quad (4.4)$$

where p_c is the confining pressure, p is the pore pressure and n is the effective-stress coefficient. This coefficient differs for different rocks and can also be a function of the confining and pore pressures, and it is generally $n \leq 1$. Some authors assume $n = 1$ (e.g. Zimmermann 1991), meaning that the

effective pressure equals the differential pressure (Terzaghi 1943). The effective-stress coefficient can also be estimated by fitting experimental velocities measured on core samples or from well logs.

We compute the dry-rock moduli as a function of the pore pressure by using the following functional forms (Carcione et al. 2003)

$$\begin{aligned} K_{sm}(z, p) &= \psi_K [1 - \exp(-p_e(p)/p_K^*)], \quad \mu_{sm}(z, p) \\ &= \Psi_\mu \left[1 - \exp\left(-p_e(p)/p_\mu^*\right) \right], \end{aligned} \quad (4.5)$$

where $\Psi_K = \beta K_{smHS}$, $\Psi_\mu = \beta \mu_{smHS}$, β is an empirical coefficient, p_K^* and p_μ^* are obtained from calibration, and K_{smHS} and μ_{smHS} are the Hashin–Shtrikman upper bounds.

4.3 Effective-Fluid Model for Partial Saturation

The properties of a fluid mixture can be computed from the properties of the single constituents, their relative concentrations and spatial distribution within the rock. Batzle and Wang (1992) provide equations to compute the compressibility, density and viscosity of water, brine and methane. Alternatively, the compressibility and density of gaseous phases at in-situ conditions can be estimated with equations of state (EOS), such as the van der Waals and Peng-Robinson equations (e.g. Carcione et al. 2006; Peng and Robinson 1976). The gas viscosity can be obtained with a formulation proposed by Luo and Vasseur (1996) or with the Lohrenz-Bray-Clark method (e.g. Danesh 1998).

At the pore scale, with a homogeneous distribution of fluids in a partially saturated medium (e.g. water and gas), the effective bulk modulus K_f is given by the isostress Wood averaging (Wood 1941). However, when partial patchy saturation occurs, fluids are generally distributed in the sediment volume involving many pores. In this case, an upper limit of K_f is the isostrain Voigt averaging (Voigt 1928). The Wood and Voigt models are the lower and upper bounds for multiphase mixtures; a more realistic equation has been provided by Brie et al. (1995):

$$K_f = K_g + (K_w - K_g) S_w^e, \quad (4.6)$$

where e is an empirical constant. If $e = 1$, the Brie formula is equivalent to the Voigt averaging, while it predicts values close to the Wood average for $e = 40$. We consider $e = (f_0/f)^{0.36}$, where f_0 is a reference frequency. Data from

the seismic to ultrasonic band can be fitted with an exponent of 0.36.

The density of the fluid mixture is

$$\rho_f = S_g \rho_g + S_w \rho_w, \quad (4.7)$$

where ρ_g and ρ_w are the gas and water densities, respectively.

Moreover, the viscosity of the fluid mixture can be obtained as (Teja and Rice 1981a, b)

$$\eta_f = \eta_g \left(\frac{\eta_w}{\eta_g} \right)^{S_w}, \quad (4.8)$$

where η_g and η_w are the gas and water viscosities, respectively.

Panel (a) of Fig. 4.1 shows an example of the fluid-mixture viscosity as a function of water saturation obtained with Eq. (4.8), where we consider $\eta_w = 1.798$ cP and $\eta_g = 0.021$ cP. For comparison, we also plot the viscosity computed with the linear law $\eta_f = S_w \eta_w + S_g \eta_g$, which overestimates the effective viscosity. Panel (b) shows the bulk modulus of the fluid mixture as a function of water saturation and frequency, based on Eq. (4.6), assuming $K_w = 2.4$ GPa, $K_g = 7.0$ MPa, and $f_0 = 5$ MHz. At low frequencies, Brie's model (Brie et al. 1995) is in good agreement with Wood model (black dashed line).

4.4 Permeability

The permeabilities of the sediment and gas hydrates frames, required by the TPB model, can be computed as a function of the pore and confining pressures and relative permeabilities as (Gangi 1981)

$$\begin{aligned} k_{sm} &= k_{s0} \left[1 - \left(\frac{p_d}{p_1} \right)^m \right]^3 (k_{rw} S_w + k_{rg} S_g), \\ k_{hm} &= k_{h0} \left[1 - \left(\frac{p_d}{p_1} \right)^m \right]^3 (k_{rw} S_w + k_{rg} S_g), \end{aligned} \quad (4.9)$$

where, k_{s0} is the rock-frame permeability in absence of gas hydrates, k_{h0} is the permeability of the gas-hydrate matrix in absence of fluids and p_d is the differential pressure, i.e. the effective pressure (Eq. 4.4). This assumes that the effective stress coefficient is 1 for the permeabilities, and that p_1 and $0 \leq m \leq 1$ are constants. The relative permeabilities k_{rw} and k_{rg} can be obtained as (Van Genuchten 1978)

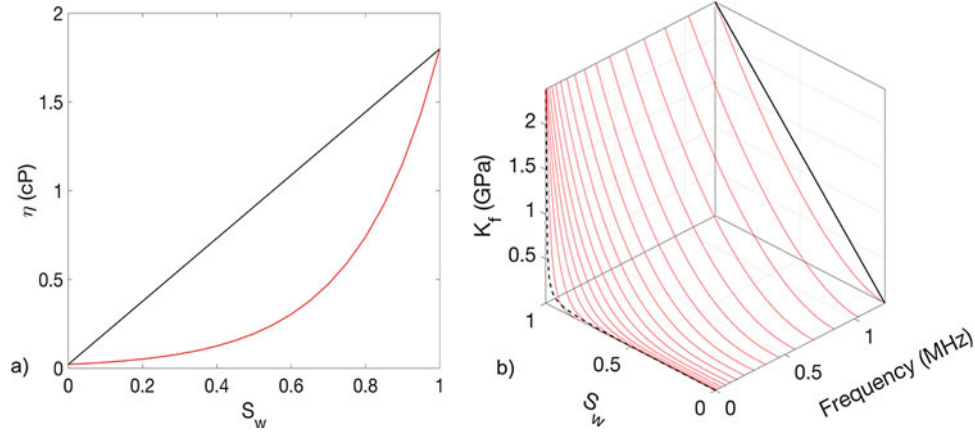


Fig. 4.1 **a** Viscosity of the fluid mixture computed with Eq. (4.8) (red) and with a linear law (black) as a function of water saturation; **b** Bulk modulus of the fluid mixture computed with Brie model

(Eq. (4.6)) as a function of saturation and frequency (red), compared with results from the Voigt model (black continuous line) and Wood model (black dashed line)

$$k_{rw} = \sqrt{S_{we}} \left[1 - \left(1 - S_{we}^{1/0.8} \right)^{0.8} \right]^2, \text{ with } S_{we} = \frac{S_w - S_{wg}}{1 - S_{wg}} \quad (4.10)$$

and

$$k_{rg} = \sqrt{S_{ge}} \left[1 - \left(1 - S_{ge}^{1/1.8} \right)^{1.8} \right]^2, \text{ with } S_{ge} = \frac{S_g - S_{gw}}{1 - S_{gw}}. \quad (4.11)$$

S_{wg} and S_{gw} are the residual saturations of gas in water and water in gas, respectively.

Figure 4.2a shows an example of normalized relative permeabilities computed with Eqs. (4.10) and (4.11) as a function of water saturation, with $S_{wg} = 0.2$ and $S_{gw} = 0.02$; there is practically no water flow for $S_w < 0.5$. Panel (b) shows an example of the rock-frame permeability (Eq. 4.9) as a function of water saturation and differential

pressure, where $k_{s0} = 10^{-13} \text{ m}^2$, $p_1 = 14 \text{ MPa}$ and $m = 0.26$ (Gangi 1981). k_{sm} decreases rapidly with increasing differential pressure.

4.5 Attenuation

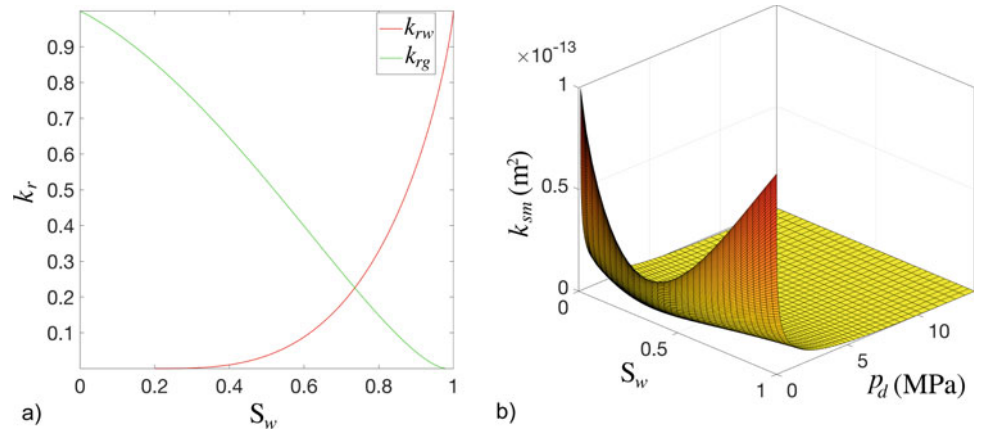
To model attenuation in gas-hydrate and free-gas bearing sediments we rely on a constant-Q model, a simple but effective viscoelasticity theory. Attenuation is implemented by making complex the frame moduli

$$K_{sm} \rightarrow K_{sm} M(\omega, Q_K) \text{ and } \mu_{smh} \rightarrow \mu_{smh} M(\omega, Q_\mu), \quad (4.12)$$

where M represents the attenuation kernel given by

$$M(\omega, Q) = \left(\frac{i\omega}{\omega_0} \right)^{2\gamma}, \quad \gamma = \frac{1}{\pi} \tan^{-1} \left(\frac{1}{Q} \right), \quad (4.13)$$

Fig. 4.2 **a** Normalized relative permeabilities as a function of water saturation; **b** and rock-frame permeability as a function of water saturation and differential pressure



where ω is the angular frequency and ω_0 is a reference frequency. In Eq. (4.12), Q_K and Q_μ are the quality factors related to the bulk and shear moduli, given by

$$Q_K = \frac{K_{sm}(z, p)}{K_{sm}(z)} Q_0 \text{ and } Q_\mu = \frac{\mu_{smh}(z, p)}{K_{sm}(z, p)} Q_K, \quad (4.14)$$

where Q_0 is a loss parameter of the frame, and $K_{sm}(z)$ is the dry-rock bulk modulus at depth z at hydrostatic pressure.

The model results in a decrease of seismic wave attenuation with increasing gas-hydrate concentration. It follows that increasing the volume fraction of a stiff material (e.g. gas hydrate) and reducing the water saturation allows for grain cementation to increase the sediment cohesion, consequently reducing the attenuation.

4.6 Seismic Velocities

The three-phase Biot theory is described in detail in Carcione and Tinivella (2000) and Gei and Carcione (2003). We outline the formulation here to obtain the seismic velocities. The theory predicts three compressional waves, one of which is fast and two of which are slow, and two shear waves, wherein one is fast and the other is slow. The phase velocity of the three compressional waves are

$$V_{Pi} = \left[\text{Re} \left(\sqrt{\Lambda_i} \right) \right]^{-1}, \quad i = 1, 2, 3, \quad (4.15)$$

where Re denotes the real part and the Λ_i are obtained by solving

$$\begin{aligned} & A\Lambda^3 \\ & - [B + C + D - 2E + 2F]\Lambda^2 + [bR_{11} + cR_{22} + dR_{33} - 2e + 2f]\Lambda \\ & - a \\ & = 0. \end{aligned} \quad (4.16)$$

The two S-wave phase velocities are

$$V_{Si} = \left[\text{Re} \left(\sqrt{\Omega_i} \right) \right]^{-1}, \quad i = 1, 2, \quad (4.17)$$

where the Ω_i are the solution of

$$\begin{aligned} & \Omega^2 \rho_{22} (\mu_{11} \mu_{33} - \mu_{13}^2) \\ & - \Omega (\mu_{11} b - \mu_{33} d - 2\mu_{13} \rho_{13} \rho_{22} + 2\mu_{13} \rho_{12} \rho_{23}) + a. \end{aligned} \quad (4.18)$$

The coefficients in Eqs. (4.16) and (4.18) are

$$\begin{aligned} A &= R_{11}R_{22}R_{33} - R_{23}^2R_{11} - R_{12}^2R_{33} - R_{13}^2R_{22} + 2R_{12}R_{23}R_{13}, \\ B &= \rho_{11}(R_{22}R_{33} - R_{23}^2), \quad C = \rho_{22}(R_{11}R_{33} - R_{13}^2), \quad D = \rho_{33}(R_{11}R_{22} - R_{12}^2), \\ E &= R_{11}R_{23}\rho_{23} + R_{33}R_{12}\rho_{12} + R_{22}R_{13}\rho_{13}, \quad F = R_{12}R_{13}\rho_{23} + R_{23}R_{12}\rho_{13} + R_{23}R_{13}\rho_{12}, \end{aligned}$$

$$\begin{aligned} a &= \rho_{11}\rho_{22}\rho_{33} - \rho_{23}^2\rho_{11} - \rho_{12}^2\rho_{33} - \rho_{13}^2\rho_{22} + 2\rho_{12}\rho_{23}\rho_{13}, \\ b &= \rho_{22}\rho_{33} - \rho_{23}^2, \quad c = \rho_{11}\rho_{33} - \rho_{13}^2, \quad d = \rho_{11}\rho_{22} - \rho_{12}^2, \\ e &= \rho_{11}\rho_{23}\rho_{23} + \rho_{33}\rho_{12}\rho_{12} + \rho_{13}\rho_{22}\rho_{13}, \quad f = \rho_{12}\rho_{13}\rho_{23} + \rho_{23}\rho_{12}\rho_{13} + \rho_{13}\rho_{23}\rho_{12}, \\ R_{11} &= K_1 + \frac{4}{3}\mu_{11}, \quad R_{12} = C_{12}, \quad R_{22} = K_2 \\ R_{13} &= C_{13} + \frac{2}{3}\mu_{13}, \quad R_{23} = C_{23}, \quad R_{33} = K_3 + \frac{4}{3}\mu_{33} \end{aligned}$$

μ_{ij} are shear coefficients

$$\begin{aligned} \mu_{11} &= [(1 - g_1)\phi_s]^2 \mu_{av} + \mu_{smh}, \\ \mu_{13} &= (1 - g_1)(1 - g_3)\phi_s\phi_h\mu_{av}, \\ \mu_{33} &= [(1 - g_3)\phi_h]^2 \mu_{av} + \mu_{hm}, \end{aligned} \quad (4.19)$$

with the average shear modulus given by

$$\mu_{av} = \left[\frac{(1 - g_1)\phi_s}{\mu_s} + \frac{\phi_f}{i\omega\eta_f} + \frac{(1 - g_3)\phi_h}{\mu_h} \right]^{-1}, \quad (4.20)$$

where $i = \sqrt{-1}$, η_f is the fluid viscosity (4.8) and

$$g_1 = \mu_{smh}/\phi_s\mu_s, \quad g_3 = \mu_{hm}/\phi_h\mu_h. \quad (4.21)$$

C_{12} , C_{13} and C_{23} are off-diagonal coupling moduli given by

$$\begin{aligned} C_{12} &= (1 - c_1)\phi_s\phi_fK_{av}, \\ C_{13} &= (1 - c_1)(1 - c_3)\phi_s\phi_hK_{av}, \\ C_{23} &= (1 - c_3)\phi_h\phi_fK_{av}, \end{aligned} \quad (4.22)$$

where c_1 and c_3 are consolidation coefficients of the rock and ice frames

$$c_1 = K_{sm}/\phi_sK_s, \quad c_3 = K_{hm}/\phi_hK_h, \quad (4.23)$$

and K_{av} is the average bulk modulus

$$K_{av} = \left[\frac{(1-c_1)\phi_s}{K_s} + \frac{\phi_f}{K_f} + \frac{(1-c_3)\phi_h}{K_h} \right]^{-1}. \quad (4.24)$$

The diagonal coupling moduli are

$$\begin{aligned} K_1 &= [(1-c_1)\phi_s]^2 K_{av} + K_{sm}, \\ K_2 &= \phi_f^2 K_{av}, \\ K_3 &= [(1-c_3)\phi_h]^2 K_{av} + K_{hm}. \end{aligned} \quad (4.25)$$

ρ_{ij} are mass density coefficients given by

$$\begin{aligned} \rho_{11} &= a_{13}\phi_s\rho_s + (a_{12}-1)\phi_f\rho_f + (a_{31}-1)\phi_h\rho_h - ib_{11}/\omega, \\ \rho_{12} &= -(a_{12}-1)\phi_f + ib_{11}/\omega, \\ \rho_{13} &= -(a_{13}-1)\phi_s\rho_s - (a_{31}-1)\phi_h\rho_h, \\ \rho_{22} &= (a_{12}+a_{23}-1)\phi_f\rho_f - i(b_{11}+b_{33})/\omega, \\ \rho_{23} &= -(a_{23}-1)\phi_f\rho_f + ib_{33}/\omega, \\ \rho_{33} &= (a_{13}-1)\phi_s\rho_s + (a_{23}-1)\phi_f\rho_f + a_{31}\phi_h\rho_h - ib_{33}/\omega. \end{aligned} \quad (4.26)$$

where a_{ij} are tortuosity coefficients. Assuming spherical pores, Leclaire et al. (1994) obtain

$$\begin{aligned} a_{12} &= \frac{1}{2} \left(\frac{\phi_s \frac{\phi_f\rho_f + \phi_h\rho_h}{\phi_f + \phi_h}}{\phi_f\rho_f} \right) + 1, & a_{13} &= \frac{1}{2} \left(\frac{\phi_h \frac{\phi_f\rho_f + \phi_s\rho_s}{\phi_f + \phi_s}}{\phi_s\rho_s} \right) + 1, \\ a_{31} &= \frac{1}{2} \left(\frac{\phi_s \frac{\phi_f\rho_f + \phi_h\rho_h}{\phi_f + \phi_h}}{\phi_h\rho_h} \right) + 1, & a_{23} &= \frac{1}{2} \left(\frac{\phi_h \frac{\phi_f\rho_f + \phi_s\rho_s}{\phi_f + \phi_s}}{\phi_f\rho_f} \right) + 1. \end{aligned} \quad (4.27)$$

b_{ii} are friction matrix coefficients, given by

$$b_{ii} = \left(\frac{\eta_f \phi_f^2}{k_i} \right) F_{i(\omega)}, \quad i = 1, 3, \quad (4.28)$$

where η_f is the fluid viscosity; $k_1 = k_{sm}$ and $k_3 = k_{hm}$ are the permeabilities of the sediment and hydrate frames (Eq. 4.9). The interaction between the rock matrix and gas-hydrate frame with the fluids is described by the viscodynamic functions $F_i(\omega)$ (Johnson et al. 1987)

$$F_i(\omega) = \sqrt{1 - \frac{4i\tau_i^2 k_i}{x_i L_i^2 \phi_f^2}}, \quad x_i = \frac{\eta_f \phi_f}{\omega k_i \rho_f}, \quad i = 1, 3, \quad (4.29)$$

where ω is the angular frequency, τ_i are tortuosities of the sediment ($\tau_1 = a_{12}$) and hydrate frame ($\tau_3 = a_{23}$) and L_i is a geometrical parameter. $2/L_i$ is the ratio between the surface and volume of the pores and $\xi_i \tau_i k_i / (\phi_f L_i^2) = 1$, ($i = 1, 3$), where ξ_i is related to the shape of the pore network, and specifically $\xi_i = 8$ for non-intersecting canted tubes and $\xi_i = 12$ for canted slabs of fluid.

4.7 Estimation of the Seismic Velocities and Attenuation

We estimate the P- and S-wave velocities and attenuation as a function of the gas-hydrate concentration and effective pressure. To calibrate the theory, we use measurements of the P-wave velocities as a function of the pore and confining pressure performed by Tobin et al. (1995) on shaly sediments from the ODP Leg 146 at site 892, Oregon accretionary prism, sample 146-892D-18X-2, 0–22 cm. We use the Hamilton (1979) empirical relationships to estimate the S-wave velocities from the P-wave velocities and compute the effective stress coefficient by regression data analysis. We obtain $n = 0.89 \exp(-0.43 p_d)$, where the differential pressure p_d is given in MPa. The elastic moduli of the sediment matrix are

$$\begin{aligned} K_{sm}(p_e)[\text{GPa}] &= 1.73 + 0.23p_e - 1.7 \exp(-p_e/0.17), \\ \mu_{sm}(p_e)[\text{GPa}] &= 0.54 + 0.06p_e - 0.54 \exp(-p_e/0.12), \end{aligned} \quad (4.30)$$

where p_e is the effective pressure provided by Eq. (4.4). The wet-rock bulk modulus is computed using the inverse Gassmann equation (e.g. Carcione 2014; Mavko et al. 2009), with porosity $\phi = 0.45$ (Westbrook et al. 1994).

Figure 4.3 shows the comparison between the measurements from Tobin et al. (1995) and the wet-rock P-wave velocities obtained with the effective pressure law.

After characterizing the sediment matrix, we use the TPB theory to estimate the seismic velocities and attenuation of the rock containing gas hydrate, water and free gas. The properties of the different constituents are given in Table 4.1, where those of methane are computed with the van der Waals equation and viscosity is obtained from the formulation proposed by Luo and Vasseur (1996). The density and incompressibility of the fluid mixture are estimated with Eqs. (4.7) and (4.6), with $f_0 = 5.46$ MHz, which is chosen to fit the patchy saturation White model velocity (White 1975; Carcione and Picotti 2006) in the absence of gas hydrate, with patches of 1 cm in diameter. The properties of the hydrate frame are obtained from Eq. (4.2) and the stiffening

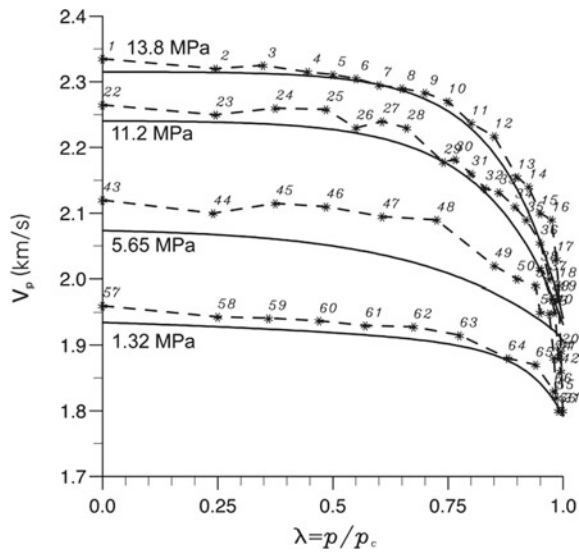


Fig. 4.3 Phase velocity V_p as a function of the overpressure ratio computed with the effective pressure law shown as a solid line, as compared to measurements from Tobin et al. (1995) shown with asterisks and dashed lines (Gei and Carcione 2003)

of the sediment skeleton due to the presence of gas hydrate with Eq. (4.3). The permeability of the sediment and hydrate frames are computed with Eqs. (4.9)–(4.11), assuming the residual saturations $S_{wg} = 0.2$ and $S_{gw} = 0.2$; $k_{s0} = 10^{-13} \text{ m}^2$ (Moran et al. 1995), $k_{h0} = 5 \times 10^{-4} \text{ m}^2$ (Leclaire et al. 1994), $p_1 = 14 \text{ MPa}$ and $m = 0.26$ (Gangi 1981). Q_K and Q_μ are estimated from equations (4.14) assuming $Q_0 = 60$ and $\omega_0 = 2\pi \text{ MHz}$. We assume that the parameter ζ of the viscodynamic functions is equal to 8 for both sediment and hydrate frames.

Figure 4.4 shows the velocity and attenuation of the P and S waves as a function of frequency and water saturation at $p_d = 0.6 \text{ MPa}$, $p_e = 3.2 \text{ MPa}$ and $\phi_h = 0.3$ (corresponding to $C_h = 0.67$). The P-wave velocity in panel (a) increases

with frequency, following the typical behavior in the transition from uniform to patchy saturation. The P-wave attenuation in panel (b) qualitatively agrees with experimental measurements reported in Murphy (1982). The Biot relaxation peak is located at about $S_w = 0.4$. The S-wave velocity shown in panel (c) increases with frequency and gas saturation $S_g = 1 - S_w$, a consequence of the decreasing bulk density. The S-wave attenuation shows a maximum at full water saturation, approximately at the location of the Biot peak.

Figure 4.5 shows the velocity and attenuation of the P waves as a function of the effective pressure and water saturation at a frequency of 30 Hz and $C_h = 0.67$. The velocity increases with effective pressure and it takes very low values for $p_e \approx 0$, corresponding to an unconsolidated sediment. The attenuation decreases for increasing effective pressure.

To the authors knowledge, estimations of gas hydrate concentration with chlorinity or other methods are not available for Site 892. However, Carcione and Gei (2004) applied the TPB theory to well log data from the Mallik site, achieving similar results to those obtained from hydrate dissociation modeling and Archie methods.

4.8 Conclusions

We present a three-phase Biot theory to estimate the P- and S-wave velocities and attenuation in partially saturated gas-hydrate bearing sediments at varying pore pressure conditions, from seismic to ultrasonic frequencies. The coexistence of gas hydrate, water and methane in the pore space is admitted and the rock-frame stiffening is accounted for by a percolation model. To illustrate the methodology, we consider a specimen of marine sediment from the Cascadia Margin, ODP Leg 146 at site 892. The elastic properties of the rock frame are obtained with an effective

Table 4.1 Material properties of the gas-hydrate bearing sediments (e.g. Mavko et al. 2009; Helgerud et al. 1999); the properties of gas correspond to the depth of the BSR at ODP Leg 146, site 892 (at hydrostatic pressure)

Sediment grain	Bulk modulus, K_s	35 GPa
	Shear modulus, μ_s	35 GPa
	Density, ρ_s	2650 kg/m^3
Gas hydrate	Bulk modulus, K_h	7.9 GPa
	Shear modulus, μ_h	3.3 GPa
	Density, ρ_h	900 kg/m^3
Water	Bulk modulus, K_w	2.4 GPa
	Density, ρ_w	1030 kg/m^3
	Viscosity, η_w	1.798 cP
Gas	Bulk modulus, K_g	7.0 MPa
	Density, ρ_g	70 kg/m^3
	Viscosity, η_g	0.021 cP

Fig. 4.4 P- and S-wave velocities are shown on panels **a**, **c** and the corresponding attenuation on panels **b**, **d** as a function of frequency and water saturation. The gas hydrate concentration is 0.67 and the differential pressure is 0.6 MPa (Gei and Carcione 2003)

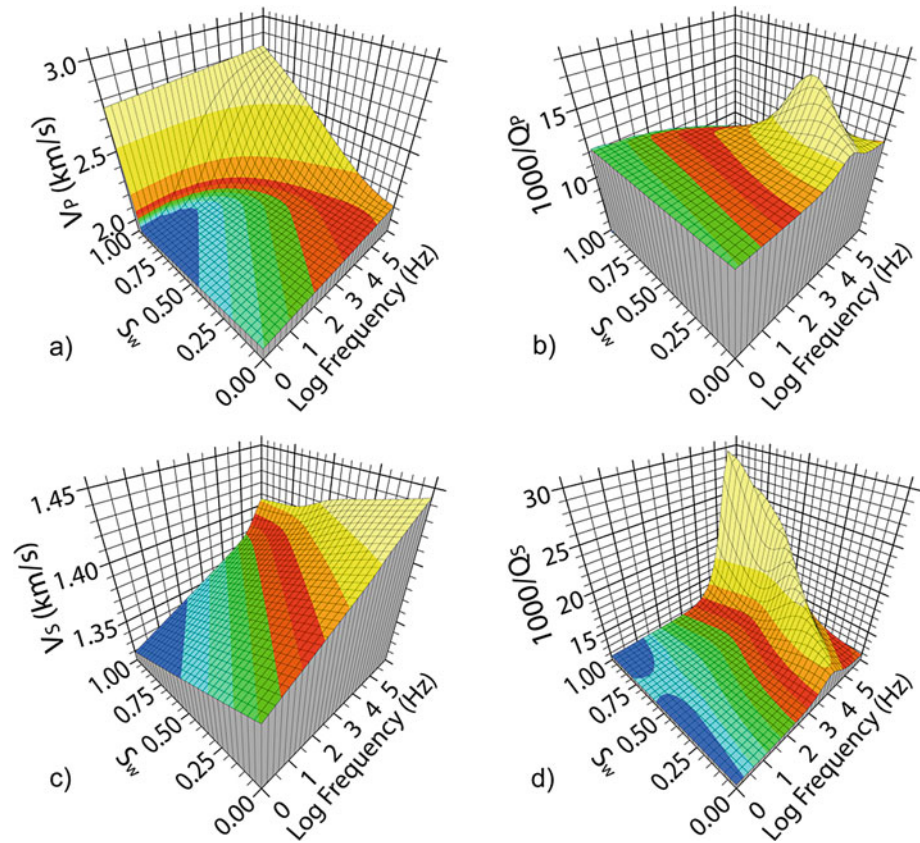
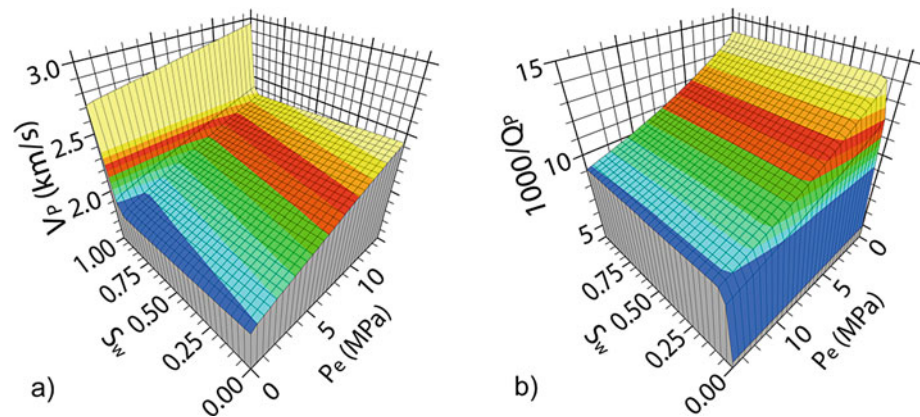


Fig. 4.5 P-wave velocity (**a**) and attenuation (**b**) as a function of water saturation and effective pressure. The gas hydrate concentration is 0.67 and the frequency is 30 Hz (Gei and Carcione 2003)



pressure law calibrated with laboratory measurements. The seismic properties at different gas-hydrate concentrations and fluid saturations are in agreement with the behavior of real sediments in many aspects. The seismic velocities increase with gas-hydrate concentration and seismic frequency. Attenuation decreases with increasing hydrate saturation and the dissipation factor (inverse Q) shows a maximum at the Biot relaxation peak, located at approximately 40% water saturation. Decreasing effective pressure leads to a strong decrease in velocity and Q factor.

References

- Arbabi S, Sahimi M (1988) Elastic properties of three-dimensional percolation networks with stretching and bond-bending forces. *Phys Rev B* 38:7173–7176
- Batzle M, Wang Z (1992) Seismic properties of pore fluids. *Geophysics* 57:1396–1408
- Biot MA (1956) Theory of propagation of elastic waves in a fluid-saturated porous solid, I: low-frequency range. *J Acoust Soc Am* 28(2):168–178
- Biot MA (1962) Mechanics of deformation and acoustic propagation in porous media. *J Appl Phys* 33(4):1482–1498

- Brie A, Pampuri F, Marsala AF et al (1995) Shear sonic interpretation in gas-bearing sands. *SPE Ann Tech Conf* 30595:701–710
- Carcione JM (2014) Wave fields in real media: wave propagation in anisotropic, anelastic, porous and electromagnetic media, 3rd edn. Elsevier, Handbook of Geophysical Exploration
- Carcione JM, Gei D (2004) Gas hydrate concentration estimated from P- and S-wave velocities at the Mallik 2L–38 research well. Mackenzie Delta, Canada. *J Appl Geophys* 56:73–78
- Carcione JM, Gurevich B (2011) Differential form and numerical implementation of Biot's poroelasticity equations with squirt dissipation. *Geophysics* 76:N55–N64
- Carcione JM, Picotti S (2006) P-wave seismic attenuation by slow-wave diffusion. Effects inhomogeneous rock properties. *Geophysics*. 71:O1–O8
- Carcione JM, Tinivella U (2000) Bottom simulating reflectors: seismic velocities and AVO effects. *Geophysics* 65:54–67. Errata 66:984
- Carcione JM, Helle HB, Pham NH et al (2003) Pore pressure estimation in reservoir rocks from seismic reflection data. *Geophysics* 68 (5):1569–1579
- Carcione JM, Gei D, Rossi G et al (2005) Estimation of gas hydrate concentration and free-gas saturation at the Norwegian-Svalbard continental margin. *Geophys Prospect* 53(6):803–810
- Carcione JM, Picotti S, Gei D et al (2006) Physics and modelling for monitoring CO₂ storage. *Pure Appl Geophys* 163:175–207
- Carcione JM, Poletto F, Farina B et al (2018) 3D seismic modeling in geothermal reservoirs with a distribution of steam patch sizes, permeabilities and saturations, including ductility of the rock frame. *Phys Earth Planet Inter* 279:67–78
- Danesh A (1998) PVT and phase behavior of petroleum reservoir fluids. Elsevier
- Gangi A (1981) The variation of mechanical and transport properties of cracked rock with pressure. In: Einstein HH (ed) *Rock mechanics from research to application*. Proceedings of the 22nd US symposium on rock mechanics, pp 85–89
- Gei D, Carcione JM (2003) Acoustic properties of sediments saturated with gas hydrate, free gas and water. *Geophys Prospect* 51:141–157
- Hamilton E (1979) Vp/Vs and Poisson's ratios in marine sediments and rocks. *J Acoust Soc Am* 66:1093–1101
- Hashin Z, Shtrikman S (1963) A variational approach to the theory of the elastic behavior of multiphase materials. *J Mech Phys Solids* 11:127–140
- Helgerud M, Dvorkin J, Nur A et al (1999) Elastic-wave velocity in marine sediments with gas hydrates: Effective medium modeling. *Geophys Res Lett* 26(13):2021–2024
- Johnson DL, Koplik J, Dashen R (1987) Theory of dynamic permeability and tortuosity in fluid-saturated porous media. *J Fluid Mech* 176:379–402
- Krief M, Garat J, Stellingwerff J et al (1990) A petrophysical interpretation using the velocities of p and s waves (full-waveform sonic). *The Log Analyst* 31(06)
- Kuster GT, Toksöz MN (1974) Velocity and attenuation of seismic waves in two-phase media: Part I. Theoretical formulations. *Geophysics* 39(5):587–606
- Leclaire Ph, Cohen-Tènoudji F, Aguirre-Puente J (1994) Extension of Biot's theory of wave propagation to frozen porous media. *J Acoust Soc Am* 96:3753–3768
- Luo X, Vasseur G (1996) Geopressuring mechanism of organic matter cracking: numerical modeling. *AAPG Bull* 80:856–874
- Murphy WF III (1982) Effects of partial water saturation on attenuation in Massilon sandstone and Vycor porous glass. *J Acoust Soc Am* 71 (6):1458–1468
- Mavko G, Mukerji T, Dvorkin J (2009) *The rock physics handbook*, 3rd edn. Cambridge University Press
- Milkov AV, Dickens GR, Claypool GE et al (2004) Co-existence of gas hydrate, free gas, and brine within the regional gas hydrate stability zone at Hydrate Ridge (Oregon margin): evidence from prolonged degassing of a pressurized core. *Earth Planet Sci Lett* 222:829–843
- Moran K, Gray WGD, Jarrett CA. (1995) Permeability and stress history of sediment from the Cascadia margin. In: Carson B, Westbrook GK, Musgrave RJ, Suess E (Ed) *Proceedings of the ocean drilling program*. *Sci Results* 146(1):275–279
- Peng DY, Robinson DB (1976) A new two-constant equation of state. *Ind Eng Chem Fundam* 15(1):59–64
- Qian J, Wang X, Collett TS et al (2018) Downhole log evidence for the coexistence of structure II gas hydrate and free gas below the bottom simulating reflector in the South China Sea. *Mar Pet Geol* 98:662–674
- Sahoo SK, Marin-Moreno H, North LJ et al (2018) Presence and consequences of coexisting methane gas with hydrate under two phase water-hydrate stability conditions. *J Geophys Res Solid Earth* 123(5):3377–3390
- Teja AS, Rice P (1981a) Generalized corresponding states method for viscosities of liquid mixtures. *Ind Eng Chem Fundam* 20:77–81
- Teja AS, Rice P (1981b) The measurement and prediction of the viscosities of some binary liquid mixtures containing n-hexane. *Chem Eng Sci* 36:7–10
- Terzaghi K (1943) *Theoretical soil mechanics*. Wiley, New York
- Tobin HJ, Moore JC, Moore G (1995) Laboratory measurement of velocity versus effective stress in thrust faults of the Oregon accretionary prism: implications for fault zone overpressure. In: *Proceedings of the ocean drilling program*. *Sci Results* 146:349–358
- van Genuchten MT (1978) Calculating the unsaturated hydraulic conductivity with a closed form analytical model. Report 78-WR-08: Princeton University, NJ
- Voigt W (1928) *Lehrbuch der kristallphysik*: Teubner
- Westbrook G, Carson B, Musgrave R et al (1994) Site 892. In: *Proceedings of the ocean drilling program*, 146
- White JE (1975) Computed seismic speeds and attenuation in rocks with partial gas saturation. *Geophysics* 40:224–232
- Wood AW (1941) *A textbook of sound*. McMillan Co, New York
- Zimmermann RW (1991) *Compressibility of sandstones*. Elsevier Science Publishing Co